Journal of Environmental Chemical Engineering 5 (2017) 5540–5546

Contents lists available at ScienceDirect

Journal of Environmental Chemical Engineering

journal homepage: www.elsevier.com/locate/jece

Research paper

Selective photodegradation of phenol in the presence of a commercial humic acid

Magdalena Palacio[a], Lucía Rossi[b], María Estefanía Farías Hermosilla[a], Janina A. Rosso[a], Paula I. Villabrille[b], Marcela V. Martin[c,*]

[a] Instituto de Investigaciones Fisicoquímicas Teóricas y Aplicadas (INIFTA, CONICET/UNLP), Facultad de Ciencias Exactas, Universidad Nacional de La Plata, Casilla de Correo 16, Sucursal 4, 1900, La Plata, Argentina
[b] Centro de Investigación y Desarrollo en Ciencias Aplicadas (CINDECA, CONICET/UNLP), Facultad de Ciencias Exactas, Universidad Nacional de La Plata, 1900, La Plata, Argentina
[c] Instituto de Desarrollo Tecnológico para la Industria Química (INTEC, CONICET/UNL), Universidad Nacional del Litoral, 3000, Santa Fe, Argentina

ARTICLE INFO

Keywords:
Photocatalysis
Cerium
Doped titanium dioxide
Controlled porosity

ABSTRACT

Preferential oxidation of certain pollutants has been a major challenge in photocatalysis, since normal source water contains low concentrations of highly toxic substances along with high concentrations of natural organic matter. Pure TiO_2 and doped with cerium (0.1 nominal at.%) by the sol–gel method under different conditions were synthesized. In one of the synthesis conditions, a nonionic surfactant was used as a pore-directing agent along with an acetic acid-based sol–gel route without addition of water molecules. The effect of the presence of a surfactant, the doping with cerium, the light absorption, the adsorption and the degradation of phenol and a commercial humic acid, as well as the structural properties of the synthesized materials, were investigated in this study.

It can be demonstrated that by controlling the porous structure of TiO_2, the access of large size natural organic matter to the TiO_2 can be suppressed, thus improving the selective oxidation of small size target contaminants. Phenol as a target contaminant was successfully decomposed even in the presence of a commercial humic acid as competing natural organic matter. Under UV irradiation, highly porous catalysts prepared with polyoxyethylene (20) sorbitan monooleate surfactant exhibited a higher photocatalytic activity for the degradation of phenol in the presence of a commercial humic acid than the materials prepared without this surfactant. Under visible irradiation, the material prepared with the surfactant and doped with Ce presented the best performance, probably due to the red shift of the electronic absorption band induced by cerium incorporation to TiO_2.

1. Introduction

The synthesis of TiO_2 catalysts mainly composed of the anatase photoactive crystalline phase, with high surface area, has been studied in recent decades for its widespread use in environmental remediation such as the photocatalytic destruction of toxic organic compounds and inactivation of microorganisms in water and air [3,18].

Reactions photocatalyzed by TiO_2 are nonselective oxidations. The rate of degradation of a wide variety of molecules is similar, because it is governed by free radical reaction mechanisms. Furthermore, this low catalyst selectivity means that the contaminant could not be treated without taking into account the rest of the compounds present in the matrix [14,11]. For example, effluents contain low concentrations of pollutant (highly toxic substances) along with high concentrations of natural organic matter (NOM) that can act as scavengers of the reactive species that are generated on the surface of TiO_2 [34,23]. Long et al. [20] claim that a major challenge for photocatalytic water purification withTiO_2 is the strong inhibitory effect of NOM. The use of TiO_2 with a mesoporous structure to restrict the access of large NOM molecules could be an attractive strategy to address this inhibitory effect.

To the best of our knowledge, only [34] evaluated the application of mesoporous TiO_2 photocatalyst to improve the selective oxidation of an organic pollutant in water. They reported the TiO_2 synthesis by the sol-gel method using a surfactant to control its porous structure. It was shown that with this material, the access to the pores of a humic acid ($C_{187}H_{186}O_{89}N_9S$; 4012 g mol^{-1}) can be suppressed and thus improve the selective oxidation of ibuprofen ((*RS*)-2-(4-(2-methylpropyl)phenyl) propanoic acid). The mass transfer is controlled in the porous TiO_2 by a size exclusion mechanism: it facilitates mass transfer of the contaminants with access to the pores and decreases the availability for the

* Corresponding author.
E-mail address: mmartin@intec.unl.edu.ar (M.V. Martin).

http://dx.doi.org/10.1016/j.jece.2017.10.021
Received 8 August 2017; Received in revised form 5 October 2017; Accepted 10 October 2017
Available online 12 October 2017
2213-3437/

larger NOM.

A surfactant is a substance with an amphiphilic nature, so it is often used in a sol-gel synthesis as a pore-directing agent. In this way, it allows the control of the size and shape of particles to improve the material properties, producing highly porous materials with specific pore size and structure [1]. Several researchers focus their studies on the modification of the textural characteristics of TiO_2 by the presence of an organic "template" during the synthesis by the sol-gel method [7,8,5,4,13,28,25,21,34]. In all cases, an improvement in the degradation of the studied pollutants (generally dyes such as methylene blue and methyl orange) was reported. In most studies, a single surfactant was used, and only in some cases the effect of the surfactant concentration was studied [6,4,25].

Although the effect of the presence of a surfactant on the textural properties of the materials was known, only [34] evaluated the selectivity in the degradation of a contaminant by the simultaneous presence of other compounds.

Previously, we studied the enhancement of TiO_2 photocatalysis by cerium doping for phenol degradation [24,22]. Although we reached good values for phenol degradation, the photocatalytic experiments were performed in ultrapure water. Therefore, further studies should be done to mimic real water matrices.

Although the efficiency of different treatments for phenol degradation has been reviewed by several authors [12,19,15], as far as we know there are no reports about the influence of Ce-doped TiO_2 on the photodegradation of phenol in the presence of NOM.

The goal of our study is to find photocatalysts able to degrade phenol even in the presence of NOM.

Here we present a comparative study on the photocatalytic efficiency of undoped and Ce-doped TiO_2 (0.1 nominal atomic %) prepared by the sol–gel method under different conditions. One of the syntheses was performed with the addition of a nonionic surfactant as a structure director. The synthesized catalysts were characterized by X-ray diffraction, UV–vis diffuse reflectance spectra, and N_2 physisorption. The photocatalytic activity of the materials for the oxidative degradation of phenol in the presence of a commercial humic acid was investigated.

2. Experimental section

2.1. Chemicals

The following reagents were used: isopropanol (*i*-PrOH, Biopack), polyoxyethylene (20) sorbitan monooleate (Tween 80, Aldrich), absolute ethanol (Anedra), nitric acid (Anedra), acetic acid (Anedra), phenol (Aldrich), and humic acid (Aldrich). The metal-ion precursors of Ce and Ti were cerium(III) nitrate hexahydrate ($Ce(NO_3)_3{\cdot}6H_2O$, Aldrich) and titanium tetraisopropoxide (TTIP, Aldrich), respectively.

2.2. Preparation of photocatalysts

2.2.1. Synthesis I

In a recent paper, we reported a sol-gel synthesis of cerium-doped TiO_2 [24]. An ethanolic TTIP solution (1:10 (v/v)) was added dropwise to an acid aqueous solution (50 mL of distilled water adjusted to pH 1) under vigorous stirring at 25 °C. Then, the TiO_2 sol was continuously stirred for 24 h, and the resulting suspension was evaporated and dried overnight at 50 °C. The crystals were ground to powder and calcined at 600 °C (6 °C min^{-1}) for 1 h, under air. The undoped sample was white and it will be referred to hereafter as **I** (undoped). Ce-doped TiO_2 was prepared according to the above procedure using $Ce(NO_3)_3\ 6H_2O$ as cerium precursor. An appropriate amount of this salt was dissolved and mixed with the acid aqueous solution before the hydrolysis of TTIP. The subsequent procedures were the same as described above. The Ce-doped powder with a doping level of 0.1 nominal atomic % (at. %) exhibited a yellow tone. This material will be referred to hereafter as **I-Ce** (referring to the metal added as dopant).

2.2.2. Synthesis II

Pure and Ce-doped TiO_2 particles were also obtained by an acetic acid-based sol–gel route without direct addition of water molecules.

The TiO_2 particles were prepared by the following procedure: an isopropyl alcoholic TTIP solution (where 5 mL of TTIP was mixed with 15 mL of *i*-PrOH) was added dropwise to an isopropyl alcoholic acid solution (26 mL of *i*-PrOH with 6 mL of acetic acid) under strong stirring at 25 °C. Acetic acid was added to the solution for the *in situ* generation of water through the esterification reaction with alcohol. This reaction helps to control the hydrolysis and condensation reactions of TTIP [32]. The molar ratio of *i*-PrOH:acetic acid:TTIP was 33:6:1. The resulting gel was dried at 55 °C overnight. The obtained crystals were washed with water three times, then dried and ground to powder, and calcined at 600 °C (6 °C min^{-1}) for 1 h.

Ce-doped TiO_2 was prepared according to the above procedure in the presence of $Ce(NO_3)_3\ 6H_2O$. The needed amount of cerium precursor to give a doping level of 0.1 nominal at. % was added to the isopropyl alcoholic acid solution, and the subsequent steps were the same as described in the previous paragraph. The prepared materials will be referred to hereafter as **II** (undoped) and **II-Ce** (referring to the metal added as dopant).

2.2.3. Synthesis II with nonionic surfactant

The catalysts were prepared by the sol–gel method with the addition of a surfactant modifying the procedure reported by [7]. Tween 80 was selected as a representative nonionic long chain amphiphilic molecule. This organic pore-directing agent has several advantages compared to other commonly used toxic and ionic templating agents; it is relatively inexpensive, biodegradable, nontoxic, and easily removable. Besides, this surfactant was characterized by an ordered mesophase and the ability to synthesize tailor-designed porous TiO_2 catalytic materials [7]. The surfactant was diluted in an isopropyl alcoholic acid solution. Then, TTIP diluted in *i*-PrOH was added dropwise under vigorous stirring. The molar ratio of surfactant:*i*-PrOH:acetic acid:TTIP was 0.3:28:6:1. After continuous stirring for 24 h, a transparent gel with a yellow tone, homogeneous, and stable was obtained. The resulting gel was dried at 55 °C overnight. The obtained crystals were washed with water three times, then dried and ground to powder, and calcined at 600 °C (6 °C min^{-1}) for 1 h.

Ce-doped TiO_2 was prepared according to the above procedure in the presence of $Ce(NO_3)_3\ 6H_2O$. The appropriate amount of metal-ion precursor was added to *i*-PrOH before the surfactant was diluted, to give a doping level of 0.1 nominal at. %, and the subsequent procedures were the same as described above. These catalysts will be referred to hereafter as **II-Tw** (undoped) and **II-CeTw** (referring to the addition of cerium and Tween 80), as indicated in Table 1.

2.3. Characterization of the photocatalysts

In order to study the crystalline structure of the synthesized catalysts, a Philips diffractometer (PW-1390) with Cu Kα radiation (λ = 1.5417 Å) and Ni filter for values of 2θ between 20° and 80° was employed. For the determination of the Brunauer-Emmett-Teller (BET) surface area and porosity of the materials, adsorption-desorption isotherms of N_2 at 77 K were obtained using a Micromeritics ASAP 2020 surface area and porosity analyzer. The study of the optical properties of the solid samples was carried out by UV–vis diffuse reflectance, with a UV–vis spectrophotometer Perkin-Elmer Lambda 35 with an

Table 1
Synthesized catalysts nomenclature.

Catalyst	Synthesis I	Synthesis II	Synthesis II-Tw
undoped	I	II	II-Tw
Ce-doped	I-Ce	II-Ce	II-CeTw

integrating sphere attachment.

2.4. Photocatalytic decomposition of pollutant

A cylindrical glass batch reactor was used to carry out the photocatalytic oxidation of phenol in the presence of AHA at 25 °C. The reaction mixture for each of the tests was prepared by ultrasonically dispersing (in the dark for 15 min) 0.47 mg phenol, 100 mg catalyst, 1.2 mg AHA, and 100 mL ultrapure water (< 20 ppb organic carbon and resistivity > 18 MΩ cm). These experimental conditions were selected according to previous experiments with catalyst **I**. The initial amount of AHA was 12 mg L^{-1} because it is the average concentration usually reported for natural waters [2]. All experiments were performed at mixture inherent pH (around 6). The mixture was kept under uninterrupted stirring to maintain the catalyst in suspension, and the reactor was kept open to air to get sufficient oxygen for the photochemical reaction. A Rayonet RPR-100 model photochemical reactor purchased from Southern New England Ultraviolet Company, with eight UV lamps (with maximum at 365 nm) or Vis lamps (with maximum at 575 nm), was used. The lamp-spectrum and irradiation pattern in/inside the reactor were previously reported [22]. Spectral irradiance employed in the experiments was measured with a high-resolution Avantes spectrometer (AvaSpec-ULS3648 model). The radiative flux values were determined as 28 ± 1 and 20 ± 1 W m^{-2} for the UV and Vis lamps, respectively.

The samples were taken periodically, then filtered by 0.45 μm and stored in amber glass bottles in a refrigerator until analysis. An HPLC, Hewlett–Packard (HP) 1050 Ti series, and the corresponding standard solutions were used to determine the phenol concentration in the samples. A reversed-phase C18 (4.6 mm x id 250 mm, particle size 5 μm) Restek Pinnacle II was used as column with a mixture of methanol/H_3PO_4 (0.2%) 50/50 (v/v) as eluent at 0.8 mL min^{-1} constant flux.

The total organic carbon (TOC) was determined by a high-temperature carbon analyzer model TOC 5000A from Shimadzu, using a calibration curve with standard solutions of potassium hydrogen phthalate. The detection limits were 1 ppm C. These measurements were carried out for a more effective evaluation of the degree of mineralization reached by all organic compounds in the mixture (phenol, AHA, and all possible reaction intermediates).

The photolysis of phenol and AHA was evaluated as control experiments. For this purpose, the evolution of phenol concentration in aqueous solution and the degree of mineralization with irradiation (without catalyst) were analyzed. The adsorption of phenol and AHA on the materials was also checked, by monitoring the evolution of phenol concentration and TOC without irradiation (with each catalyst).

3. Results and discussion

3.1. Catalyst characterization

Fig. 1 shows XRD patterns of synthesized TiO_2 catalysts. The crystalline phases were identified by comparison with the International Center for Diffraction Data (ICDD), JCPDS ID Numbers 89-4921 and 04-0551 for anatase and rutile, respectively. A complete anatase to rutile phase transformation was observed at 600 °C for catalyst **I**. Meanwhile, the presence of two polymorphs, anatase (83 wt%) and rutile (17 wt%), was detected for catalyst **II**, synthesized without direct addition of water. These results indicate that the conditions of the synthesis alter the crystalline properties of the material. Under synthesis II conditions, it was possible to stabilize the anatase phase up to 600 °C.

For catalyst **I-Ce**, both crystalline phases were also detected at this temperature. However, for **II-Tw**, **II-CeTw** and **II-Ce**, only the anatase phase was observed after the same heat treatment. It could be concluded that cerium doping and Tween 80 addition inhibited the anatase-rutile phase transformation up to 600 °C.

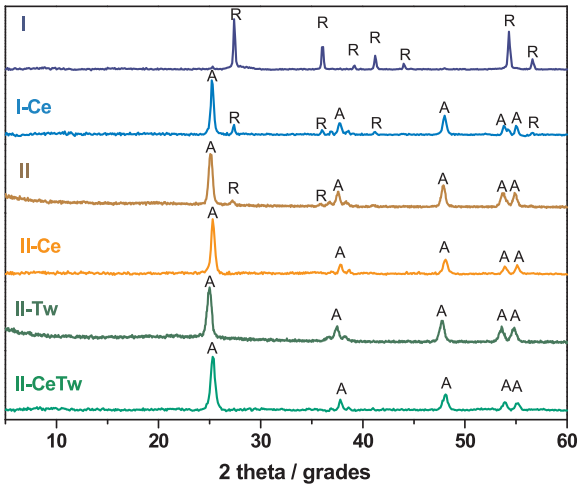

Fig. 1. XRD patterns of synthesized TiO_2 catalysts (calcined at 600 °C) R:Rutile, A:Anatase.

Yurtsever and Çiftçioğlu [33] studied some rare earth (RE) element-doped TiO_2 powders. They concluded that the anatase to rutile phase transformation was inhibited by RE doping. In particular, they suggested that stabilization of the Ti-O bond by Nd doping may lead to a decrease in the atomic mobility, which may also lead to the inhibition of the anatase to rutile phase transformation.

The effect of the surfactant addition on TiO_2 phase transformation was also investigated by Choi et al. (2007b). They observed that the anatase–rutile phase transformation occurred at around 550 °C for a catalyst synthesized without surfactant, but when surfactant was added, only the anatase phase was present even at 600 °C. They concluded that the addition of surfactants suppressed the phase transformation significantly. Our results are in line with these findings.

No diffraction peaks that could be attributed to the dopant ion were observed for **II-Ce** and **II-CeTw**, in accordance with our previous report for **I-Ce** [24]. That is because the doping level and the thermal treatment employed were similar even though some other conditions of sol-gel synthesis changed (*in situ* water formation and/or surfactant addition). However, it could also be that metal species formed during the synthesis are well dispersed on the TiO_2 surface or are too small to be detected by the equipment used [9,16].

For the rutile (110) peak and the anatase (101) peak, the X-ray diffraction intensities and broadening were analyzed. From the diffraction peak broadening and using the Scherrer equation [17], Eq. (1)) the average size of TiO_2 crystallites was estimated.

$$D = K\lambda/\beta \cos\theta \quad (1)$$

D: the average crystallite diameter in angstrom;

B: the line width at half-maximum height of the main intensity diffraction peak of anatase (101) or rutile (110) after background removal;

$K = 0.89$: a constant related to the crystallite shape and the way in which D and β are defined;

θ: the diffraction angle;

λ: the X-ray wavelength corresponding to CuKα irradiation (1.5417 Å).

The Spurr-Myers equation [10] was used to determine the weight percent of the anatase and rutile phases:

$$A\ wt\% = (1 + 1.265 I_R/I_A)^{-1} \times 100 \quad (2)$$

$$R\ wt\% = 100 - A\ wt\% \quad (3)$$

where I_A and I_R are the diffraction intensities of the (101) anatase and (110) rutile crystalline phases at $2\theta = 25.3°$ and 27.5°, respectively.

Table 2 lists the values of the crystallite sizes of anatase and rutile

Table 2
Structural and optical properties of synthesized photocatalysts calcined at 600 °C.

Catalyst	XRD				UV–vis	
	Crystallite size[a] (nm)		Crystalline phase[b] (wt%)		E_{GAP} (eV)	Wavelength (nm)
	Anatase	Rutile	Anatase	Rutile		
I[c]	n.d.	98.47	n.d.	100.00	3.07	404
I-Ce[c]	23.86	84.40	81.00	19.00	2.80	443
II	28.30	14.67	83.00	17.00	3.02	410
II-Ce	19.25	n.d.	100.00	n.d.	2.65	468
II-Tw	28.22	n.d.	100.00	n.d.	3.12	397
II-CeTw	15.47	n.d.	100.00	n.d.	2.70	460

[a] Estimated by Scherrer equation using the XRD line broadening.
[b] Weight percentages of anatase and rutile were calculated by Spurr-Myers equation.
[c] Reported by [24].

phases with their respective weight percentages.

The crystallite size of anatase thus estimated for titania obtained by synthesis **II** (without surfactant) decreases from 28.30 nm (**II**) to 19.25 nm (**II-Ce**) with the addition of Ce. The crystallite growth of titania could be inhibited through the formation of Ce—O—Ti bonds, because of the presence of Ce^{3+} ions on the particle surfaces at grain boundaries and grain junctions, which results in an increase in the diffusion barrier at the TiO_2 grain junctions [29].

The anatase crystallite size for Ce-doped titania from synthesis **II** decreases from 19.25 nm (**II-Ce**) to 15.47 nm (**II-CeTw**) when Tween 80 is used. Anatase particles are formed by crystallization of amorphous particles and grow by three possible pathways as follows: (1) direct aggregation of amorphous particles, (2) solid-state aggregation of anatase particles, and (3) atom-by-atom recrystallization of anatase particles. During heat treatment, the remaining organics are believed to inhibit the natural stages for the crystallization and solidification of TiO_2 material by surrounding TiO_2 grains. This can also explain how the surfactants can act as a crystallite size inhibitor by obstructing the growth and nucleation of adjacent anatase grains [7].

Additionally, of the three materials (**II-Ce, II-Tw and II-CeTw**) that contain only the anatase phase, the one with the smallest crystal size is **II-CeTw**, which was obtained in synthesis **II** with addition of Ce and Tween 80. Therefore, both effects contribute to a decrease in the size of anatase crystals.

The absorption spectra of the samples were evaluated by UV–vis DRS. Table 2 lists the band gap energy (E_{GAP}) values of the photocatalysts. The E_{GAP} of the materials was estimated using Eq. (4) [35]:

$$(\alpha h\nu)^n = B\,(h\nu - Eg) \quad (4)$$

where:

$h\nu$: the photon energy,

α: the absorption coefficient that can be obtained from the scattering and reflectance spectra according to the Kubelka–Munk theory,

B: a constant relevant to the material, and

n: the value that depends on the nature of transition: 2 for a direct allowed transition, 3/2 for a direct forbidden transition, and 1/2 for an indirect allowed transition. Then, the absorption E_{GAP} value was obtained by extrapolation at $\alpha = 0$ when $(\alpha h\nu)^n$ ($n = 1/2$) versus $h\nu$ was represented.

The E_{GAP} values for the undoped TiO_2 are in the range of 3.02–3.12 eV, i.e., between the E_{GAP} for anatase and rutile of 3.2 and 3.0 eV, respectively [27]. For the catalysts synthesized, the E_{GAP} is not substantially modified by the type of synthesis employed (*in situ* water formation and/or surfactant addition). However, with the addition of cerium a significant modification is generated, and the E_{GAP} values of doped catalysts are in the range of 2.6–2.8 eV. A red shift of the electronic absorption band was induced by cerium incorporation to TiO_2. We demonstrated in previous work that the magnitude of that shift depends on the amount of Ce added [24].

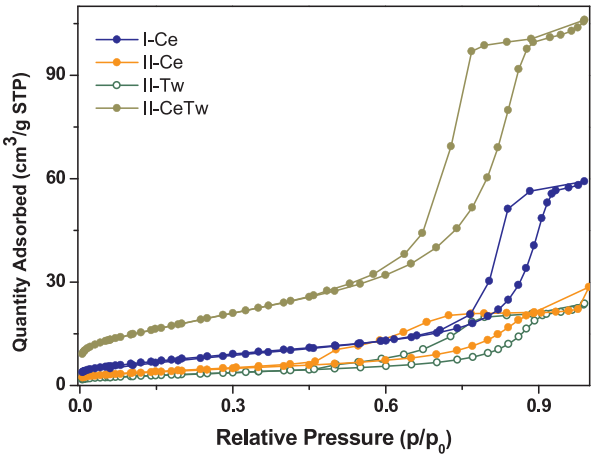

Fig. 2. N_2 sorption isotherms at 77 K of synthesized photocatalysts calcined at 600 °C.

The physisorption isotherms for the doped materials synthesized with or without surfactant, which are shown in Fig. 2, exhibited typical type IV behavior with a hysteresis loop, according to the IUPAC classification [31]. These isotherms have a well-defined adsorption curve step between relative pressures P/P_0 of 0.4–0.9 and large hysteresis loops due to capillary condensation associated with uniform cylindrical mesopores. According to [26], the hysteresis loop at medium relative pressure (P/P_0 = 0.4–0.7) resulting from the condensation within the framework-confined mesopores is typical of mesoporosity, while that at high partial pressure ($P/P_0 > 0.8$) is associated with textural mesoporosity. For the materials of Fig. 2, it can be said that all have both types of mesoporosity.

The specific surface area, total pore volume, and pore diameter of the materials measured from N_2 sorption analysis are summarized in Table 3. Catalysts **II** and **I**, both without doping and without surfactant, have very low specific surface areas, 1.1 and 4.8 $m^2\,g^{-1}$, respectively. Their isotherms had no hysteresis loops, therefore they cannot be classified within type IV according to the IUPAC classification [31], and for that reason their total pore volume and pore diameter were not included in Table 3.

As can be seen from Table 3, the specific surface area values were affected by the synthesis conditions. Either doping with cerium or the use of Tween 80 led to an increase in the specific surface area. Other authors [34] indicated that TiO_2 prepared in the presence of a surfactant was more thermally stable than that of the control. The thermal stability also prevented crystallite size growth.

Moreover, the highest value of specific surface area obtained for **II-CeTw** could indicate a synergistic effect of cerium and Tween 80. Decrease in the sintering rate and inhibition in crystal growth could result in the largest specific surface area observed for this material.

The BJH pore size distributions of **I-Ce**, **II-Ce**, **II-Tw** and **II-CeTw**

Table 3
Textural properties of synthesized photocatalysts calcined at 600 °C.

Catalyst	N_2 physisorption			
	Isotherm type (IUPAC)	S_{BET} ($m^2\,g^{-1}$)	Pore volume* ($cm^3\,g^{-1}$)	Pore size* (nm)
I	–	4.8	–	–
I-Ce	IV	27.7	0.090	9.7
II	–	1.1	–	–
II-Ce	IV	15.1	0.045	5.8
II-Tw	IV	11.2	0.037	6.7
II-CeTw	IV	63.7	0.165	6.9

*BJH derived from desorption branches.

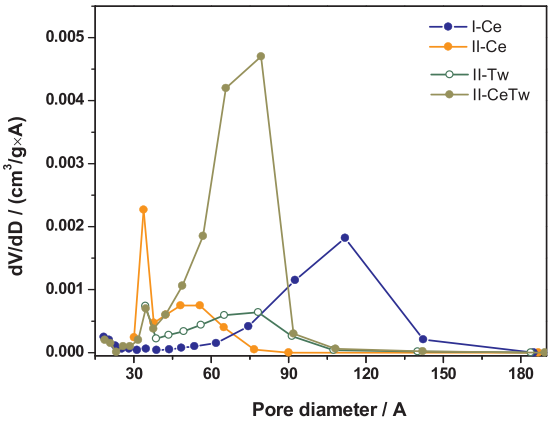

Fig. 3. BJH pore size distribution derived from desorption branches of the catalysts.

are shown in Fig. 3. The average pore diameters obtained from BJH desorption were 6.7 and 6.9 nm for **II-Tw** and **II-CeTw**, respectively. It can be assumed that in the presence of Tween 80 the catalysts have nearly the same pore size (about 7 nm) and the same pore size distribution, as expected from the type of synthesis employed. Moreover, the pore size distribution of **II-CeTw** was very narrow, implying good homogeneity of the pores. However, for the materials synthesized without surfactant, different pore size distributions were observed.

3.2. Photocatalytic degradation of phenol in the presence of AHA

To evaluate the possible photolysis of phenol or AHA, three aqueous solutions (50 μM phenol, 12 mg L^{-1} AHA, and 50 μM phenol with 12 mg L^{-1} AHA) were irradiated with UV or Vis lamps (without catalyst) for 3 or 5 h, respectively. The systems were monitored by HPLC and TOC. In all cases, the degradation was less than 5%, and no mineralization was detected.

In the presence of the synthesized catalysts, without irradiation (in the dark), differences between experimental and analytical phenol concentrations were observed after 3 h, indicating adsorption of phenol on these materials. Phenol adsorption for all systems was less than 10%.

Experiments of photocatalytic degradation of phenol in the presence of AHA using UV (3 h) or Vis lamps (5 h) were done. Fig. 4 shows the percentage of phenol degradation and mineralization.

In a previous report [24], **I and I-Ce** materials were studied in detail. The catalyst **I-Ce** showed higher efficiency for the degradation of phenol (approximately 93%) than the undoped TiO_2 (**I**), with UV irradiation. However, in the present work for **I-Ce** in the presence of AHA only 55% of phenol was degraded. This result confirms the inhibitory effect of AHA on the photocatalytic degradation of phenol.

The materials obtained in the absence of surfactant show an improvement when doped with cerium (**I-Ce** and **II-Ce**). This lanthanide ion could act as an effective electron scavenger to trap the bulk electrons in TiO_2 as a consequence of its known redox pair (Ce^{3+}/Ce^{4+}) [30]. On the other hand, the increase in surface area (see Table 3) also contributes to improving the photocatalytic performance.

However, no differences in the performance of the degradation were observed between doped and undoped materials synthesized in the presence of Tween 80. The catalysts **II-Tw** and **II-CeTw** exhibited the highest efficiency for the degradation of phenol in the presence of AHA (see Fig. 4).

The main effect on textural properties due to the use of the surfactant was that these catalysts have nearly the same pore size (about 7 nm) and the same pore size distribution. This aspect of the materials seems to be more relevant than the differences in surface area, due to the doping with Ce.

As previously discussed, the presence of cerium extends the photoresponse of the materials into the visible region (see Table 2), and this can lead to an increase in the charge separation efficiency of surface electron-hole pairs. For catalysts **II-Tw** and **II-CeTw**, the E_{GAP} values correspond to 397 and 460 nm, respectively. For the experiments with UV lamps (with maximum at 365 nm) these differences appear to be unimportant. Then, experiments using Vis lamps (with maximum at 575 nm) were performed. Under Vis lamp irradiation, phenol degradation in the presence of AHA was 34% for **II-CeTw**, while for **II-Tw** the percent degradation is negligible (within experimental error). As expected, these values are significantly lower than the ones obtained using UV lamps. However, due to the relevance of visible light in the solar spectrum, these values are promising results.

Under irradiation with UV lamps, for both materials (**II-CeTw** and **II-Tw**) the degradation of phenol could be described as an exponential trend (Fig. 5), with the same apparent rate constant of (2.5 ± 0.5) 10^{-4} s^{-1} (r^2 = 0.98). Phenol degradation under irradiation with Vis lamps for **II-CeTw** also follows an exponential trend, but with a lower apparent rate constant of (1.1 ± 0.4) 10^{-4} s^{-1} (r^2 = 0.97).

For all the cases, the observed mineralization was similar to or lower than the degradation of phenol (see Fig. 4), indicating the formation of organic compounds as a consequence of the photocatalytic process. These compounds could be produced from phenol, AHA, or both. A more detailed study has to be done to test the toxicity of the final reaction mixture.

4. Conclusion

It can be concluded that the incorporation of Tween 80 in the material: (i) increases the transition temperature for anatase to rutile phase transformation, (ii) confines the crystallite size of anatase phase, (iii)

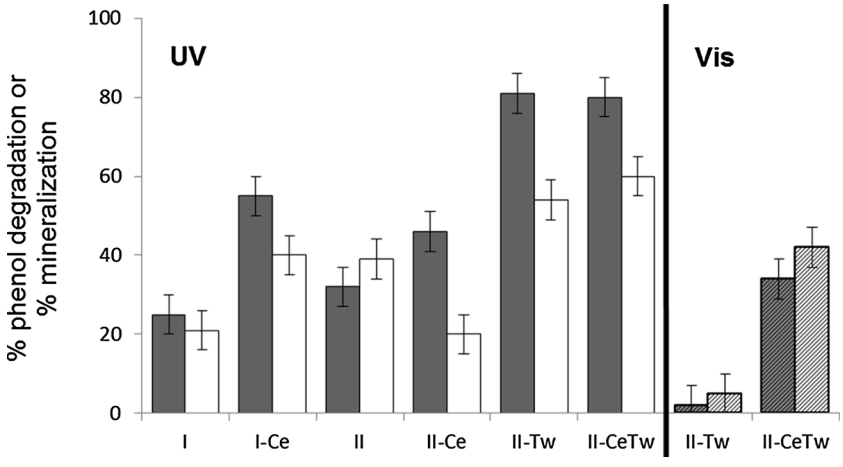

Fig. 4. Percentage of phenol degradation (gray bars) and percentage of mineralization (white bars) for the experiments with the prepared catalysts, after irradiation with UV lamps (plain bars) or Vis lamps (dashed bars), for 3 h or 5 h, respectively. Reaction conditions: catalyst = 1.0 g L^{-1}, $[phenol]_0$ = 50 μM, 12 mg L^{-1} AHA.

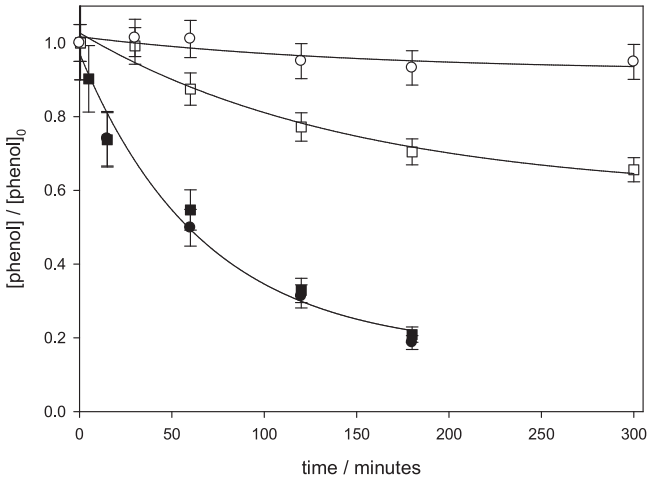

Fig. 5. Phenol degradation in the presence of catalysts **II-Tw** (circles) or **II-CeTw** (squares), with UV lamp (black symbols) or Vis lamp (white symbols) irradiation. Reaction conditions: catalyst = 1.0 g L^{-1}, $[phenol]_0$ = 50 μM, 12 mg L^{-1} AHA.

increases the specific surface area, and (iv) controls pore size and distribution.

Under UV lamp irradiation, only the pore size seems to dominate the photoactivity of these materials. The catalysts with higher efficiency for the degradation of phenol in the presence of Aldrich humic acids correspond to II-Tw and II-CeTw.

However, with Vis lamp irradiation II-CeTw presented better performance than II-Tw, probably due to the red shift of the electronic absorption band induced by cerium incorporation to TiO_2.

It is noteworthy that although the selective phenol degradation with II-CeTw under Vis lamp irradiation was quite low (34%), it is a promising material because of its potential applicability under solar exposure conditions.

Acknowledgments

M.P. and L.R. thank Consejo Nacional de Investigaciones Científicas y Técnicas (CONICET, Argentina) for fellowships. P.I.V., J.A.R. and M.V.M. are research members of CONICET. Authors wish to thank the financial support of the following Argentinean Institutions: Universidad Nacional de La Plata and FONCyT (PICT-2013-2830). The authors would especially like to thank P. Fetsis for his experimental contribution to adsorption-desorption isotherms of N_2 measurements.

References

[1] A.L. Anderson, R. Binions, The Effect of tween® surfactants in sol-gel processing for the production of TiO_2 thin films, Coatings 4 (4) (2014) 796–809, http://dx.doi.org/10.3390/coatings4040796.

[2] M. Beck, O. Dellwig, S. Fischer, B. Schnetger, H.-J. Brumsack, Trace metal geochemistry of organic carbon-rich watercourses draining the NW German coast, Estuarine Coastal Shelf Sci. 104–105 (66–79) (2012), http://dx.doi.org/10.1016/j.ecss.2012.03.025.

[3] F. Bosc, A. Ayral, P.-A. Albouy, C. Guizard, A simple route for low-temperature synthesis of mesoporous and nanocrystalline anatase thin films, Chem. Mater. 15 (12) (2003) 2463–2468, http://dx.doi.org/10.1021/cm031025a.

[4] Y. Chen, D.D. Dionysiou, Bi modal mesoporous TiO_2-P25 composite thick films with high photocatalytic activity and improved structural integrity, Appl. Catal. B: Environ. 80 (1-2) (2008) 147–155, http://dx.doi.org/10.1016/j.apcatb.2007.11.010.

[5] H. Choi, E. Stathatos, D.D. Dionysiou, Photocatalytic TiO_2 films and membranes for the development of efficient wastewater treatment and reuse systems, Desalination 202 (1-3) (2007) 199–206, http://dx.doi.org/10.1016/j.desal.2005.12.055.

[6] H. Choi, E. Stathatos, D.D. Dionysiou, Effect of surfactants in sol on TiO_2 photocatalyst, Top. Catal. 44 (4) (2007) 513–521, http://dx.doi.org/10.1007/s11244-006-0099-1.

[7] H. Choi, E. Stathatos, D.D. Dionysiou, Synthesis of nanocrystalline photocatalytic TiO_2 thin films and particles using sol-gel method modified with nonionic surfactants, Thin Solid Films 510 (1-2) (2006) 107–114, http://dx.doi.org/10.1016/j.tsf.2005.12.217.

[8] H. Choi, A.C. Sofranko, D.D. Dionysiou, Nanocrystalline TiO_2 photocatalytic membranes with a hierarchical mesoporous multilayer structure: synthesis, characterization, and multifunction, Adv. Funct. Mater. 16 (8) (2006) 1067–1074, http://dx.doi.org/10.1002/adfm.200500658.

[9] J. Choi, H. Park, M.R. Hoffmann, Effects of single metal-ion doping on the visible-light photoreactivity of TiO_2, J. Phys. Chem. C 114 (2010) 783–792, http://dx.doi.org/10.1021/jp908088x.

[10] K. Demeestere, J. Dewulf, T. Ohno, P. Herrera Salgado, H. Van Langenhove, Visible light mediated photocatalytic degradation of gaseous trichloroethylene and dimethyl sulfide on modified titanium dioxide, Appl. Catal. B: Environ. 61 (2005) 140–149, http://dx.doi.org/10.1016/j.apcatb.2005.04.017.

[11] H. Dong, G. Zeng, L. Tang, C. Fan, C. Zhang, X. He, Y. He, An overview on limitations of TiO_2-based particles for photocatalytic degradation of organic pollutants and the corresponding countermeasures, Water Res. 79 (2015) 128–146, http://dx.doi.org/10.1016/j.watres.2015.04.038.

[12] S. Esplugas, J. Gimenez, S. Contreras, E. Pascual, M. Rodriguez, Comparison of different advanced oxidation processes for phenol degradation, Water Res. 36 (2002) 1034–1042, http://dx.doi.org/10.1016/S0043-1354(01)00301-3.

[13] O.L. Galkina, V.V. Vinogradov, A.V. Agafonov, A.V. Vinogradov, Surfactant-Assisted Sol-Gel Synthesis of TiO_2 with uniform particle size distribution, Int. J. Inorg. Chem. 2011 (2011) 1–8, http://dx.doi.org/10.1155/2011/108087.

[14] U.I. Gaya, A.H. Abdullah, Heterogeneous photocatalytic degradation of organic contaminants over titanium dioxide: a review of fundamentals, progress and problems, Photoch. Photobiol. C 9 (1) (2008) 1–12, http://dx.doi.org/10.1016/j.jphotochemrev.2007.12.003.

[15] E. Grabowska, J. Reszczynska, A. Zaleska, Mechanism of phenol photodegradation in the presence of pure and modified-TiO_2: a review, Water Res. 46 (2012) 5453–5471, http://dx.doi.org/10.1016/j.watres.2012.07.048.

[16] S.N.R. Inturi, T. Boningari, M. Suidan, P.G. Smirniotis, Visible-light-induced photodegradation of gas phase acetonitrile using aerosol-made transition metal (V, Cr, Fe, Co, Mn, Mo, Ni, Cu, Y, Ce, and Zr) doped TiO_2, Appl. Catal. B Environ. 144 (2014) 333–342, http://dx.doi.org/10.1016/j.apcatb.2013.07.032.

[17] H.P. Klug, L.E. Alexander, X-Ray Diffraction Procedures: For Polycrystalline and Amorphous Materials, 2nd edn, Wiley, New York, 1974.

[18] M. Koelsch, S. Cassaignon, C. Ta Thanh Minh, J.-F. Guillemoles, J.-P. Jolivet, Electrochemical comparative study of titania (anatase, brookite and rutile) nanoparticles synthesized in aqueous medium, Thin Solid Films 451 (-452) (2004) 86–92, http://dx.doi.org/10.1016/j.tsf.2003.11.150.

[19] L.F. Liotta, M. Gruttadauria, G. Di Carlo, G. Perrini, V. Librando, Heterogeneous catalytic degradation of phenolic substrates: catalysts activity, J. Hazard. Mater 162 (2009) 588–606, http://dx.doi.org/10.1016/j.jhazmat.2008.05.115.

[20] M. Long, J. Brame, F. Qin, J. Bao, Q. Li, J.J. Alvarez, Phosphate changes effect of humic acids on TiO_2 photocatalysis: from inhibition to mitigation of electron-hole recombination, Environ. Sci. Technol. 51 (2017) 514–521, http://dx.doi.org/10.1021/acs.est.6b04845.

[21] E.G. Mariquit, W. Kurniawan, Hinode H. MiyauchiM, Effect of addition of surfactant to the surface hydrophilicity and photocatalytic activity of immobilized Nano-TiO_2 thin films, J. Chem. Eng. Jpn. 48 (10) (2015) 856–861, http://dx.doi.org/10.1252/jcej.14we421.

[22] M.V. Martin, A. Ipiña, P.I. Villabrille, J.A. Rosso, Combination of sunlight, oxidants, and Ce-doped TiO_2 for phenol degradation, Environ. Sci. Pollut. R 24 (7) (2017) 6013–6021, http://dx.doi.org/10.1007/s11356-016-6258-4.

[23] M.V. Martin, G.T. Ruiz, M.C. Gonzalez, C.D. Borsarelli, D.O. Mártire, Photolytic and radiolytic oxidation of humic acid, Photochem. Photobiol. 88 (4) (2012) 810–815, http://dx.doi.org/10.1111/j.1751-1097.2012.01116.x.

[24] M.V. Martin, P.I. Villabrille, J.A. Rosso, The influence of Ce doping of titania on the photodegradation of phenol, Environ. Sci. Pollut. R 22 (18) (2015) 14291–14298, http://dx.doi.org/10.1007/s11356-015-4667-4.

[25] E.O. Oseghe, S. Maddila, G.P. Ndungu, S.B. Jonnalagadda, Effect of surfactant concentration on active species generation and photocatalytic properties of TiO_2, Appl. Catal. B: Environ. 176 (-177) (2015) 288–297, http://dx.doi.org/10.1016/j.apcatb.2015.04.010.

[26] E. Prouzet, T.J. Pinnavaia, Assembly of mesoporous molecular sieves containing wormhole motifs by a nonionic surfactant pathway: control of pore size by synthesis temperature, Angew. Chem. Int. Ed. 36 (5) (1997) 516–518, http://dx.doi.org/10.1002/anie.199705161.

[27] D.O. Scanlon, C.W. Dunnill, J. Buckeridge, Band alignment of rutile and anatase TiO_2, Nat. Mater. 12 (9) (2013) 798–801, http://dx.doi.org/10.1038/nmat3697.

[28] O. Sheikhnejad-bishe, F. Zhao, A. Rajabtabar-Darvishi, E. Khodadad, A. Mostofizadeh, Y. Huang, Influence of temperature and surfactant on the photocatalytic performance of TiO_2 Nanoparticles, Int. J. Electrochem. Sci. 9 (2014) 4230–4240.

[29] C.P. Sibu, S. Rajesh Kumar, P. Mukundan, K.G.K. Warrier, Structural modifications and associated properties of lanthanum oxide doped sol-gel nanosized titanium oxide, Chem. Mater. 14 (7) (2002) 2876–2881, http://dx.doi.org/10.1021/cm010966p.

[30] A.M.T. Silva, C.G. Silva, G. Dražić, J.L. Faria, Ce-doped TiO_2 for photocatalytic degradation of chlorophenol, Catal. Today 144 (1-2) (2009) 13–18, http://dx.doi.org/10.1016/j.cattod.2009.02.022.

[31] K.S.W. Sing, Reporting physisorption data for gas/solid systems, Pure Appl. Chem. 54 (11) (1982) 2201–2218, http://dx.doi.org/10.1351/pac198254112201.

[32] C. Wang, Z.X. Deng, Y. Li, The synthesis of nanocrystalline anatase and rutile titania in mixed organic media, Inorg. Chem. 40 (20) (2001) 5210–5214, http://dx.doi.org/10.1021/ic0101679.

[33] H.A. Yurtsever, M. Çiftçioğlu, The effect of rare earth element doping on the microstructural evolution of sol-gel titania powders, J. Alloys Compd. 695 (2016)

1336–1353, http://dx.doi.org/10.1016/j.jallcom.2016.10.275.
[34] A. Zakersalehi, M. Nadagouda, H. Choi, Suppressing NOM access to controlled porous TiO_c particles enhances the decomposition of target water contaminants, Catal. Commun. 41 (2013) 79–82, http://dx.doi.org/10.1016/j.catcom.2013.07.013.
[35] G. Zhou, H. Sun, S. Wang, H. Ming Ang, M.O. Tadé, Titanate supported cobalt catalysts for photochemical oxidation of phenol under visible light irradiations, Sep. Purif.Technol. 80 (2011) 626–634, http://dx.doi.org/10.1016/j.seppur.2011.06.021.